

## 不同空间约束壁数对激光诱导铜击穿光谱的影响

代玉银<sup>1</sup>, 于丹<sup>2</sup>, 李英华<sup>1\*</sup>, 陈安民<sup>3</sup>, 金明星<sup>3</sup><sup>1</sup>吉林大学白求恩第一医院核医学科, 吉林 长春 130021;<sup>2</sup>空军航空大学航空基础学院, 吉林 长春 130022;<sup>3</sup>吉林大学原子与分子物理研究所, 吉林 长春 130012

**摘要** 提高激光诱导击穿光谱(LIBS)的信号强度是提高 LIBS 探测灵敏度的重要途径。本文以铜靶为烧蚀样品,研究了大气环境中不同空间约束壁数(0、2、3、4)和圆柱形约束壁对激光诱导 Cu 等离子体光谱的影响,并通过 Boltzmann 图方法测量了等离子体的电子温度。实验结果表明:当使用约束壁约束 Cu 等离子体时,Cu 原子谱线强度、信背比和电子温度均比不存在约束时明显提高;随着腔体约束壁数增加,Cu 原子谱线强度、信背比和电子温度逐渐提高;当腔体约束壁为圆柱形时,Cu 原子谱线强度、信背比和电子温度最高。空间约束壁为圆柱形壁时空间约束对等离子体的约束效果最好,光谱信号最优。

**关键词** 光谱学; 激光诱导击穿光谱; 空间约束壁数; 光谱增强; 电子温度

中图分类号 O506

文献标志码 A

doi: 10.3788/CJL202249.0611001

## 1 引言

激光诱导击穿光谱(LIBS)技术是一种强大的光谱分析技术,可以直接用于分析各种材料的元素组成及含量<sup>[1-4]</sup>。LIBS 技术与原子荧光光谱法、原子吸收光谱法、电感耦合等离子体原子发射光谱法等相比,具有原位、实时、快速、安全性高、检测时间短、检测类型丰富、对检测材料微损等特点<sup>[5-6]</sup>。如今,LIBS 已被广泛应用于材料成分分析、环境监测、珠宝鉴定、空间探索和考古探测等诸多领域<sup>[7-9]</sup>。然而,传统 LIBS 技术的光谱信号相对较弱且灵敏度较低,鉴于此,人们尝试采用多种技术来增强等离子体光谱,以提高 LIBS 技术的探测灵敏度。典型的增强方法包括纳米粒子增强 LIBS<sup>[10-11]</sup>、表面增强 LIBS<sup>[12]</sup>、偏振增强 LIBS<sup>[13-14]</sup>和双脉冲 LIBS<sup>[15-19]</sup>。

相比以上技术,空间约束 LIBS 技术具有操作简单、成本低、效率高等独特优点,已被广泛应用于增强等离子体光谱。众所周知,激光脉冲烧蚀待测靶后产生激光等离子体,伴随着激光等离子体产生

的冲击波通常以超声速膨胀。膨胀的冲击波碰到腔体内壁后被反射回去,反射的冲击波会对等离子体起到压缩作用,导致等离子体内粒子之间的碰撞速率增大,增加高能状态原子的数量,进而增强等离子体辐射<sup>[20-22]</sup>。许多研究人员对空间约束进行了研究,例如:Gao 等<sup>[23]</sup>使用两块平行铝板约束 Cu 等离子体,观察到了 Cu 原子和离子光谱强度显著增强;杨雪等<sup>[24]</sup>使用平行板约束聚甲基丙烯酸甲酯(PMMA)等离子体,观察到了 CN 分子光谱强度显著提高;陈金忠等<sup>[25]</sup>使用圆形碳片约束等离子体,观察到了 Fe、Mn、K 和 Ti 的光谱强度明显提高;Shen 等<sup>[26]</sup>使用圆柱形装置约束 Al 等离子体,观察到了 Al 原子谱线强度明显增强;Guo 等<sup>[27]</sup>使用半球形装置约束 Mn 等离子体,观察到了 Mn 原子谱线强度显著增强。上述研究分别使用平行板装置、圆柱形装置和半球形装置来研究空间约束对等离子体光谱辐射的影响。相关资料显示,目前各种空间约束装置对等离子体光谱加强的对比研究尚不多见,因此,有必要对比研究不同约束壁数下等离子体

收稿日期: 2021-07-02; 修回日期: 2021-07-19; 录用日期: 2021-08-03

基金项目: 吉林省科技厅自然科学基金(20200201334JC)、国家自然科学基金(11674128,11674124,11974138)、吉林省教育厅资助项目(JJKH20200937KJ)

通信作者: \*liyinh@jlu.edu.cn

的光谱强度。

本课题组采用高度相同(8 mm)、约束壁数不同(0、2、3、4)的腔体或约束壁为圆柱形的腔体来约束 Cu 等离子体,并讨论了约束壁数对 Cu 原子谱线强度和信背比(SBR)的影响。此外,本课题组通过 Boltzmann 图方法计算了 Cu 等离子体的电子温度,并讨论了约束壁数对 Cu 等离子体电子温度的影响。

## 2 实验装置

LIBS 实验装置示意图如图 1(a)所示。脉冲激光光源为 Surelite III 调 Q Nd:YAG 激光器,脉冲宽度为 10 ns,工作波长为 1064 nm,重复频率为 10 Hz,激光脉冲能量为 45 mJ,在样品表面上的光斑直径约为 500  $\mu\text{m}$ 。激光束经聚焦透镜 L1(焦距为 100 mm)垂直聚焦到待测 Cu 靶表面。待测 Cu 靶放置在 PT3/M-Z8 三维平移台上并随其一起运动,目的是避免激光长时间辐照靶表面的同一位置。激光与 Cu 靶相互作用产生等离子体,等离子体辐射由聚焦透镜 L2(BK7,焦距为 75 mm,直径为 50 mm)收集,然后通过光纤传导至配备增强型 CCD(ICCD)的 SP-500i 光谱仪(1200 line/mm)中。光电二极管探测光阑散射的光后产生电信号,电信号通过触发

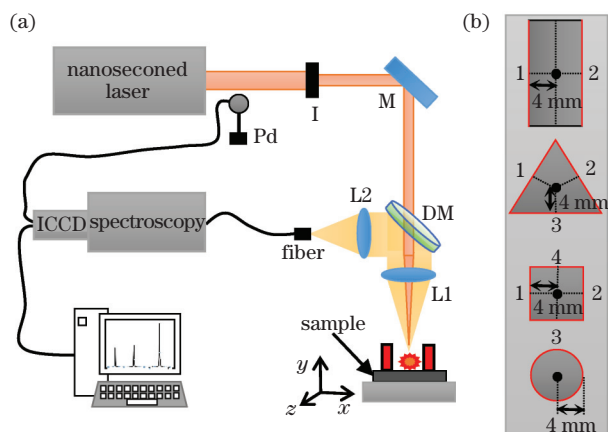


图 1 LIBS 实验装置示意图及腔体示意图。(a) LIBS 实验装置示意图(M, 反射镜; Pd, 光电二极管; DM, 双色镜; I, 光阑; L, 透镜; ICCD, 增强型 CCD); (b) 约束壁数不同(2、3、4)的腔体以及圆柱形约束壁腔体示意图

Fig. 1 Schematics of LIBS experimental setup and cavities. (a) Schematic of LIBS experimental setup (M, mirror; PD, photodiode; DM, dichroic mirror; I, iris; L, lens; ICCD, intensified CCD); (b) schematics of cavities with different numbers of confinement walls (2, 3, and 4) and cavity with cylindrical confinement wall

ICCD 相机来同步激光脉冲与 ICCD 门延迟时间。图 1 (b)显示了采用铝合金加工制作成的不同空间约束壁数(2、3、4)的空间约束腔体以及圆柱形约束腔体,两条边约束腔的腔壁到中心的距离为 4 mm,三条边约束腔中心到各边的距离均为 4 mm,四条边约束腔的腔壁到中心的距离为 4 mm,圆柱形壁的半径为 4 mm。所有约束腔的高度均为 8 mm。约束腔紧贴 Cu 靶表面,且聚焦位置位于腔体中心。每个光谱数据是 20 个光谱信号的平均值,整个实验过程在空气氛围中进行。

## 3 结果与讨论

### 3.1 光谱强度

参考原子光谱数据库,基于光谱信号强、背景信号干扰弱的原则,选取三条 Cu 原子谱线(510.55, 515.32, 和 521.82 nm)作为分析谱线<sup>[28]</sup>。图 2 显

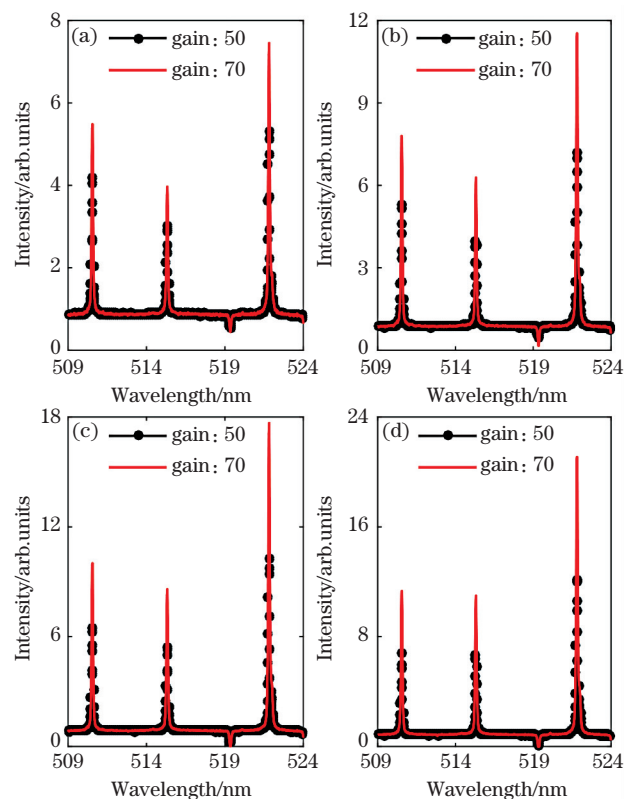


图 2 延时为 12.5  $\mu\text{s}$  时不同约束壁数下的光谱,ICCD 门宽为 0.5  $\mu\text{s}$ ,激光能量为 45 mJ。(a)约束壁数为 0; (b)约束壁数为 2;(c)约束壁数为 3;(d)约束壁数为 4

Fig. 2 Spectra for different numbers of confinement walls at delay time of 12.5  $\mu\text{s}$ . Gate width of ICCD is 0.5  $\mu\text{s}$ , and laser energy is 45 mJ. (a) Wall number is 0; (b) wall number is 2; (c) wall number is 3; (d) wall number is 4

示了延时为  $12.5 \mu\text{s}$  时不同约束壁数下的光谱, ICCD 的门宽为  $0.5 \mu\text{s}$ , 激光能量为  $45 \text{ mJ}$ 。圆点线和直线分别代表增益为 50 和 70。对比 Cu 等离子体的辐射光谱可以发现, 随着约束壁数增加, 三条 Cu (I) 原子谱线强度不断增强。此外, 增益为 70 时三条 Cu (I) 原子谱线强度明显高于增益为 50 时的谱线强度。上述结果表明, 在  $12.5 \mu\text{s}$  延时处, 空间约束对三条 Cu (I) 原子谱线强度均有着明显的增强效果。那么, 空间约束对其他延时处的谱线强度是否也具有增强效果呢? 接下来继续讨论。

图 3 显示了不同约束壁数 ( $n$ ) 下 Cu (I) 谱线在  $521.82 \text{ nm}$  处的时间分辨光谱强度, ICCD 的门宽为  $0.5 \mu\text{s}$ , 激光能量为  $45 \text{ mJ}$ 。图中圆点线是约束壁数为 0 时 Cu (I) 谱线的强度演化, 方点线是约束壁数为 2 时 Cu (I) 谱线的强度演化, 正三角线是约束壁数为 3 时 Cu (I) 谱线的强度演化, 倒三角线是约束壁数为 4 时 Cu (I) 谱线的强度演化, 菱形线是圆柱形约束壁下 Cu (I) 谱线强度的演化。由图 3 可以看出: 当约束壁数为 0 时,  $5 \sim 25 \mu\text{s}$  延迟时间内谱线强度随着延时的增加而不断衰减, 这符合长延迟时间段等离子体光谱的衰减过程<sup>[29]</sup>; 当约束壁数为 2、3、4 时以及约束壁为圆柱形壁时, Cu (I) 谱线的强度先随着采集延时的增加而衰减, 到一定延迟时间 ( $9 \mu\text{s}$ ) 时, Cu (I) 谱线强度逐渐增强, 达到最大值 ( $12.5 \mu\text{s}$ ) 后又开始衰减。激光作用于约束腔中心位置处的 Cu 靶表面产生等离子体, 伴随 Cu 等离子体产生的冲击波快速向四周膨胀 (冲击波的膨胀速度大于等离子体的扩散速度), 冲击波在膨胀过程中被约束腔体的内壁反射, 被反射的冲击波将 Cu 等离子体压缩至较小的体积。等离子体内的能量不能迅速扩散, 低能级原子吸收能量后跃迁至高能级, 导致 Cu (I) 谱线强度在  $9 \sim 20 \mu\text{s}$  的采集延时时内增强<sup>[30-32]</sup>。Li 等<sup>[33]</sup>使用快速成像技术检测了等离子体形态的演化过程, 结果发现, 在空间约束下, 随着冲击波对等离子体的压缩, 等离子体变细, 等离子体宽度减小。Gao 等<sup>[23]</sup>分别采用快速成像和阴影图像技术拍摄了等离子体的演化图像和冲击波的繁衍图像, 结果显示: 有约束壁时, 等离子体在冲击波作用下变得更窄更细了, 而且在冲击阴影图像上可以清楚地观察到从约束壁反弹回来的冲击波, 而在没有约束壁的情况下, 冲击波会以半球形膨胀。Fu 等<sup>[34]</sup>根据冲击波的繁衍图像给出了冲击波的变化过程图, 冲击波被约束壁反射, 反射回的冲击波压缩了等离子体。可见, 空间约束条件下等离子体的光

谱增强源于冲击波对等离子体的压缩, 等离子体羽中各种粒子的数密度增加, 进而增加了粒子之间的碰撞概率和等离子体温度, 光谱强度增加。

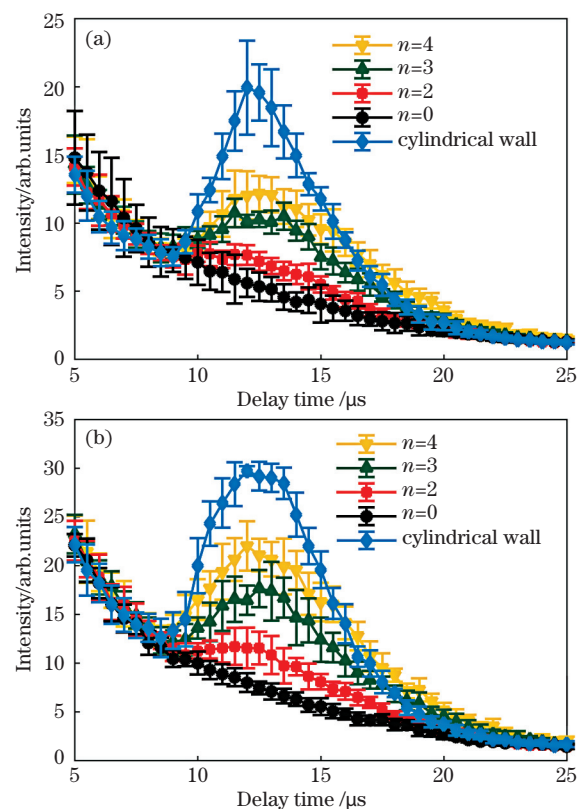


图 3 不同约束壁数下 Cu (I) 谱线在  $521.82 \text{ nm}$  处的时间分辨光谱强度, ICCD 的门宽为  $0.5 \mu\text{s}$ , 激光能量为  $45 \text{ mJ}$ 。(a) 增益为 50; (b) 增益为 70

Fig. 3 Time-resolved spectral intensity of Cu (I) line at  $521.82 \text{ nm}$  for different numbers of confinement walls. Gate width of ICCD is  $0.5 \mu\text{s}$  and laser energy is  $45 \text{ mJ}$ . (a) Gain is 50; (b) gain is 70

此外, 在  $9 \sim 22 \mu\text{s}$  的采集延时范围内, 约束壁数与 Cu (I) 谱线的峰值强度呈正相关。为了更直观地观测 Cu (I) 谱线峰值强度与约束壁数的相关性, 对比了延时为  $12.5 \mu\text{s}$  时不同约束壁数下 Cu (I)  $521.82 \text{ nm}$  谱线的增强因子, 如图 4 所示。通过对比不同约束壁数下 Cu (I) 谱线的增强因子可知, 约束壁数为 2 时, Cu (I)  $521.82 \text{ nm}$  谱线的增强因子最小, 随着约束壁数增加, 增强因子逐渐增大, 圆柱形约束壁具有最高的增强因子。为更清晰地理解这一现象, 图 5 给出了不同约束壁数下激光诱导 Cu 等离子体约束的对比示意图。图 5(a) 表示 Cu 等离子体冲击波产生并向四周膨胀, 图 5(b) 表示冲击波膨胀至腔体内壁并被反射, 图 5(c) 表示被反射的冲击波面与等离子体羽相遇, 图 5(d) 表示被反射的冲击波将等离子体压缩至较小体积。通过对比图 5

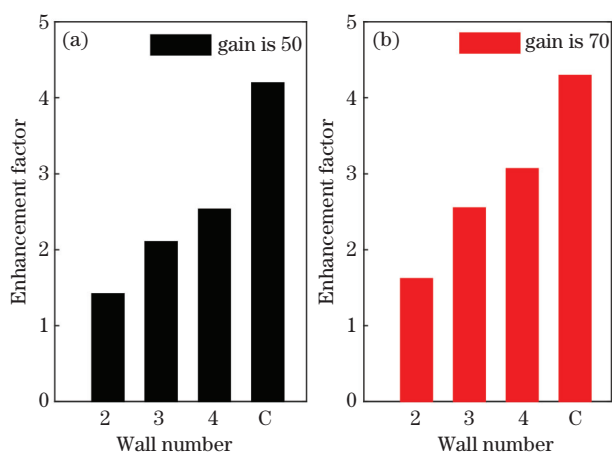


图 4 延时为  $12.5 \mu\text{s}$  时不同约束壁数(2、3、4)及圆柱形约束壁 C 下 Cu (I) 521.82 nm 谱线的增强因子对比,ICCD 的门宽为  $0.5 \mu\text{s}$ ,激光能量为 45 mJ。  
(a)增益为 50;(b)增益为 70

Fig. 4 Comparison of enhancement factor of Cu (I) line at 521.82 nm for different numbers of confinement walls and cylindrical confinement wall at delay time of  $12.5 \mu\text{s}$ . Gate width of ICCD is  $0.5 \mu\text{s}$  and laser energy is 45 mJ. (a) Gain is 50; (b) gain is 70

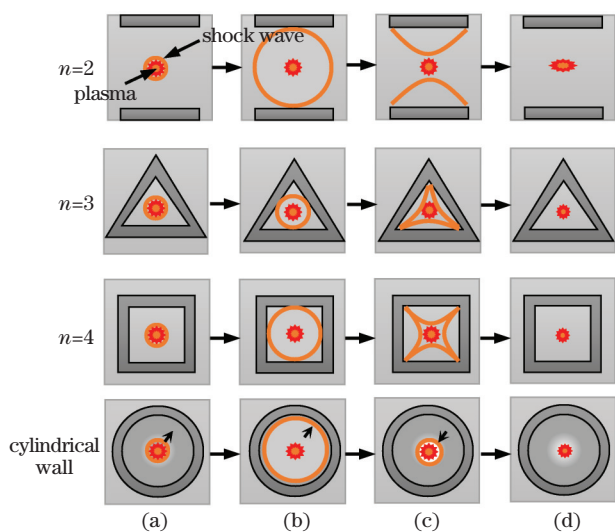


图 5 不同约束壁数下激光诱导 Cu 等离子体约束示意图对比。(a)冲击波产生;(b)冲击波反射;(c)冲击波与等离子体相遇;(d)冲击波压缩等离子体

Fig. 5 Comparison of spatially confined laser-induced Cu plasma for different numbers of confinement walls. (a) Shock wave generation; (b) shock wave reflection; (c) shock wave meets plasma; (d) shock wave compresses plasma

所示的不同约束壁数下 Cu 等离子体变化的过程可以发现:当约束壁数为 2 时,被反射的冲击波仅会被两个面的腔壁反射,用以约束等离子体的冲击波的

能量较低,并且冲击波与等离子体羽的耦合度低;当约束壁数为 3 时,被反射的冲击波会被三个面的腔壁反射;当约束壁数为 4 时,被反射的冲击波会被四个面的腔壁反射;当约束壁为圆柱形壁时,圆形约束壁几乎能完全反射球形膨胀的冲击波,冲击波与等离子体羽耦合度高。因此,约束壁为圆柱形壁时的约束效果最好,获得的等离子体辐射的增强因子最大。

### 3.2 光谱的信背比

光谱的信背比(SBR)是衡量光谱信号的一个重要指标,它是光谱信号强度与背景强度之比。图 6 为不同约束壁数下 Cu (I) 谱线在 521.82 nm 处的时间分辨信背比。当约束壁数为 0 时,信背比随着延时不断衰减;当约束壁数为 2、3、4 以及约束壁为圆柱形时,信背比先随着延时的增加而衰减,达到一定延时( $9 \mu\text{s}$ )时,信背比逐渐增强,达到最大值( $12.5 \mu\text{s}$ )之后又开始衰减。通过对比不同约束壁

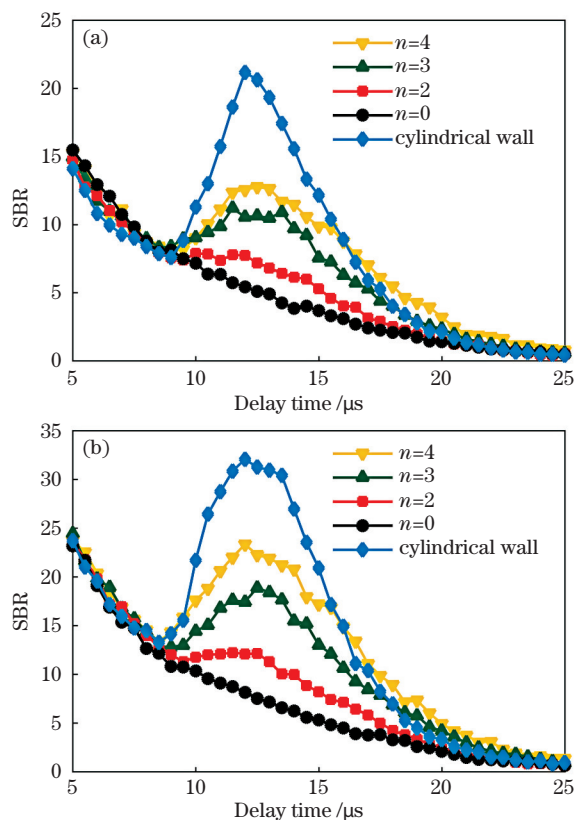


图 6 不同约束壁数下 Cu (I) 谱线在 521.82 nm 处的时间分辨信背比,ICCD 的门宽为  $0.5 \mu\text{s}$ ,激光能量为 45 mJ。(a)增益为 50;(b)增益为 70

Fig. 6 Time-resolved signal-background ratio (SBR) of Cu (I) line at 521.82 nm for different numbers of confinement walls. Gate width of ICCD is  $0.5 \mu\text{s}$  and laser energy is 45 mJ. (a) Gain is 50; (b) gain is 70

数(2、3、4)以及圆柱形约束壁下的信背比可以看出,约束壁为圆柱形时,Cu (I) 521.82 nm 谱线在 12.5 μs 处的信背比最大,其次是约束壁数为 4 时的信背比,约束壁数为 2 时的信背比最小。这表明,约束壁为圆柱形时,12.5 μs 处的光谱信号最佳。为了更深入了解空间约束对 Cu 等离子体辐射增强的机理,计算了 Cu 等离子体的电子温度。

### 3.3 电子温度

等离子体的电子温度是描述等离子体特性及理解空间约束效应的重要参数<sup>[30]</sup>。根据局部热力学平衡,等离子体温度可以从(1)式中推导出来<sup>[35-36]</sup>。

$$\ln \frac{\lambda_{mn} I_{mn}}{g_m A_{mn}} = -\frac{E_m}{k_b T} + B, \quad (1)$$

式中: $m$  和  $n$  分别是跃迁的上下能级; $A_{mn}$  是跃迁概率; $g_m$  是上能级的统计权重; $k_b$  是玻尔兹曼常数; $E_m$  是上能级的能量; $I_{mn}$  是谱线强度; $T$  为等离子体温度; $\lambda_{mn}$  是谱线波长; $B$  是截距。在当前的实验条件下,用 Cu (I) 510.55 nm、515.32 nm 和 521.82 nm 计算等离子体的电子温度。光谱参数( $E_m$ 、 $A_{mn}$  和  $g_m$ )如表 1 所示。

表 1 Cu (I)谱线的物理参数<sup>[28]</sup>

Table 1 Physical parameters of Cu (I) spectral lines<sup>[28]</sup>

Wavelength /nm	$E_m$ /eV	$g_m$	$A_{mn} / (10^8 \text{ s}^{-1})$
510.55	3.82	4	0.02
515.32	6.19	4	0.60
521.82	6.19	6	0.75

图 7 为不同约束壁数下的时间分辨 Cu 等离子体电子温度,激光能量为 45 mJ。由图 7 可以看出:当增益为 50、约束壁数为 0 时,电子温度在延时 5~25 μs 范围内逐渐下降,从 8360 K 下降到了 6199 K。当增益为 50、约束壁数为 2 时,电子温度在延时 5~9 μs 范围内逐渐下降,从 8360 K 下降到了 7839 K;在延时 9~12.5 μs 范围内,电子温度随延时增加不减反增,从 7839 K 上升到了 8010 K,并在延时 12.5 μs 时,电子温度出现一个反向增强峰;在延时 12.5~25 μs 范围内,电子温度随延时增加逐渐降低,从 8010 K 下降到了 6412 K。约束壁数为 3、4 以及圆柱形约束壁下的电子温度随延时的变化规律与约束壁数为 2 时一致。此外,增益 50 下计算的电子温度几乎等于增益 70 下计算的电子温度,这表明计算的电子温度是准确的。延时在 9 μs 之前时,伴随 Cu 等离子体产生的冲击波不断向四周膨胀,等离子体也迅速膨胀,等离子体电子温度下降;当延时大约为 9 μs 时,反射的冲击波开始压缩 Cu 等离子

体至更小的体积,等离子体密度逐渐增大,粒子之间的碰撞加剧,电子温度逐渐升高;当延时约为 12.5 μs 时,等离子体被压缩至最小体积,等离子体密度达到最大值,电子温度达到最高值;随着延时的继续增加,等离子体密度逐渐降低,电子温度也随之降低。此外,当延时为 12.5 μs 时,圆柱形约束腔中的电子温度最高,约束腔数为 0 时的电子温度最低。通过观察和分析不同约束壁数下 Cu 等离子体的光谱强度、信背比和电子温度随延时的变化可以发现,空间约束能提高光谱的辐射强度、信背比和电子温度,并且,对冲击波反射更强的腔体能使光谱强度、信背比和电子温度更高,也就是说圆柱形约束腔的空间约束效果更好。

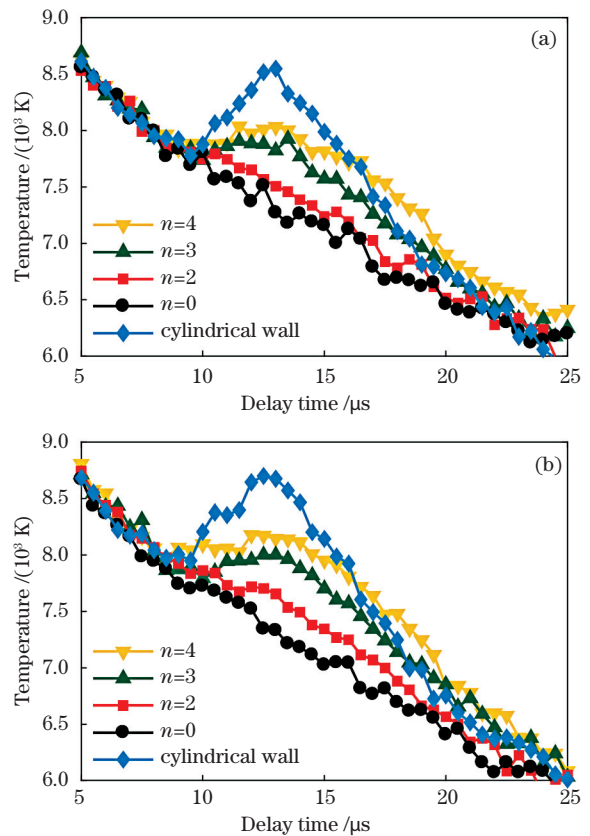


图 7 不同约束壁数下的时间分辨电子温度,ICCD 门宽为 0.5 μs,激光能量为 45 mJ。(a)增益为 50;(b)增益为 70

Fig. 7 Time-resolved electron temperature for different numbers of confinement walls. Gate width of ICCD is 0.5 μs and laser energy is 45 mJ. (a) Gain is 50; (b) gain is 70

## 4 结 论

在大气环境中研究了空间约束壁数对激光诱导 Cu 等离子体光谱的影响,结果发现:随着约束壁数

增加,Cu 原子谱线强度、信背比和电子温度均明显提高;当约束壁为圆柱形时,Cu 原子谱线强度、信背比和电子温度最高。空间约束效应来自约束腔内壁反射的冲击波对等离子体羽的压缩。随着约束壁数增加,用于约束等离子体的冲击波能量不断增强,且冲击波与等离子体羽的耦合度也不断增加,导致等离子体的压缩作用不断增强。综上可知,合适的空间约束壁能够有效提高光谱强度、信背比和电子温度,进而改善光谱信号,提高 LIBS 的探测灵敏度。

### 参 考 文 献

- [1] Jia J W, Fu H B, Wang H D, et al. Improvement of beam shape modification on stability of laser induced breakdown spectroscopy [J]. *Chinese Journal of Lasers*, 2019, 46(3): 0311004.  
贾军伟, 付洪波, 王华东, 等. 光束整形对激光诱导击穿光谱稳定性的改善[J]. *中国激光*, 2019, 46(3): 0311004.
- [2] Yang X, Zhang D, Chen A M, et al. Influence of distance between focusing lens and sample surface on atomic line and ionic line intensities of laser-induced silicon plasmas[J]. *Chinese Journal of Lasers*, 2019, 46(11): 1111001.  
杨雪, 张丹, 陈安民, 等. 聚焦透镜到样品表面的距离对激光诱导硅等离子体原子谱线强度和离子谱线强度的影响[J]. *中国激光*, 2019, 46(11): 1111001.
- [3] Wu J, Wu Y J, Fan S, et al. Signal stability of collinear double pulse laser induced breakdown spectroscopy combining with auto-focusing system [J]. *Chinese Journal of Lasers*, 2018, 45(7): 0711003.  
武进, 吴跃进, 范爽, 等. 结合自动聚焦系统的共线双脉冲激光诱导击穿光谱信号稳定性研究[J]. *中国激光*, 2018, 45(7): 0711003.
- [4] Xu W P, Chen A M, Wang Q Y, et al. Generation of high-temperature and low-density plasma with strong spectral intensity by changing the distance between the focusing lens and target surface in femtosecond laser-induced breakdown spectroscopy[J]. *Journal of Analytical Atomic Spectrometry*, 2019, 34(5): 1018-1025.
- [5] Winefordner J D, Gornushkin I B, Correll T, et al. Comparing several atomic spectrometric methods to the super stars: special emphasis on laser induced breakdown spectrometry, LIBS, a future super star [J]. *Journal of Analytical Atomic Spectrometry*, 2004, 19(9): 1061-1083.
- [6] Barbini R, Colao F, Lazic V, et al. On board LIBS analysis of marine sediments collected during the XVI Italian campaign in Antarctica [J]. *Spectrochimica Acta Part B: Atomic Spectroscopy*, 2002, 57(7): 1203-1218.
- [7] Xu X J, Wang X S, Li A Z, et al. Fast classification of tea varieties based on laser-induced breakdown spectroscopy[J]. *Chinese Journal of Lasers*, 2019, 46(3): 0311003.  
徐向君, 王宪双, 李昂泽, 等. 基于激光诱导击穿光谱的茶叶品种快速分类[J]. *中国激光*, 2019, 46(3): 0311003.
- [8] Rusak D A, Castle B C, Smith B W, et al. Fundamentals and applications of laser-induced breakdown spectroscopy [J]. *Critical Reviews in Analytical Chemistry*, 1997, 27(4): 257-290.
- [9] Harilal S S, Brumfield B E, LaHaye N L, et al. Optical spectroscopy of laser-produced plasmas for standoff isotopic analysis [J]. *Applied Physics Reviews*, 2018, 5(2): 021301.
- [10] de Giacomo A, Gaudioso R, Koral C, et al. Nanoparticle-enhanced laser-induced breakdown spectroscopy of metallic samples [J]. *Analytical Chemistry*, 2013, 85(21): 10180.
- [11] Dell'Aglio M, Alrifai R, de Giacomo A. Nanoparticle enhanced laser induced breakdown spectroscopy (NELIBS), a first review[J]. *Spectrochimica Acta Part B: Atomic Spectroscopy*, 2018, 148: 105-112.
- [12] Aguirre M A, Legnaioli S, Almodóvar F, et al. Elemental analysis by surface-enhanced laser-induced breakdown spectroscopy combined with liquid-liquid microextraction [J]. *Spectrochimica Acta Part B: Atomic Spectroscopy*, 2013, 79/80: 88-93.
- [13] Yu D, Sun Y, Feng Z S, et al. Improving emission intensity of femtosecond laser-induced breakdown spectroscopy by using circular polarization [J]. *Chinese Journal of Lasers*, 2021, 48(1): 0111001.  
于丹, 孙艳, 冯志书, 等. 通过圆偏振光提高飞秒激光诱导击穿光谱的发射强度[J]. *中国激光*, 2021, 48(1): 0111001.
- [14] Penczak J S, Liu Y M, Gordon R J. Polarization and fluence dependence of the polarized emission in nanosecond laser-induced breakdown spectroscopy [J]. *Spectrochimica Acta Part B: Atomic Spectroscopy*, 2011, 66(2): 186-188.
- [15] Lin X M, Li H, Yao Q H. Signal detection of carbon in iron-based alloy by double-pulse laser-induced breakdown spectroscopy [J]. *Plasma Science and Technology*, 2015, 17(11): 953-957.
- [16] Rashid B, Ahmed R, Ali R, et al. A comparative study of single and double pulse of laser induced breakdown spectroscopy of silver [J]. *Physics of Plasmas*, 2011, 18(7): 073301.

- [17] Chen A, Wang Y, Sui L, et al. Optical emission generated from silicon under dual-wavelength femtosecond double-pulse laser irradiation[J]. *Optics Express*, 2015, 23(19): 24648-24656.
- [18] Shen J, Yang Z C, Liu X L, et al. Analysis of enhanced laser-induced breakdown spectroscopy with double femtosecond laser pulses[J]. *Plasma Science and Technology*, 2015, 17(2): 147-152.
- [19] Sun D X, Su M G, Dong C Z, et al. A comparative study of the laser induced breakdown spectroscopy in single- and collinear double-pulse laser geometry[J]. *Plasma Science and Technology*, 2014, 16(4): 374-379.
- [20] Chen J Z, Bai J N, Song G J, et al. Enhancement effects of flat-mirror reflection on plasma radiation [J]. *Applied Optics*, 2013, 52(25): 6295-6299.
- [21] Wang X W, Chen A M, Wang Y, et al. Spatial confinement effect on femtosecond laser-induced Cu plasma spectroscopy[J]. *Physics of Plasmas*, 2017, 24(10): 103305.
- [22] Li C M, Guo L B, He X N, et al. Element dependence of enhancement in optics emission from laser-induced plasma under spatial confinement [J]. *Journal of Analytical Atomic Spectrometry*, 2014, 29(4): 638-643.
- [23] Gao X, Liu L, Song C, et al. The role of spatial confinement on nanosecond YAG laser-induced Cu plasma[J]. *Journal of Physics D: Applied Physics*, 2015, 48(17): 175205.
- [24] Yang X, Chen A M, Li S Y, et al. Effect of parallel plate constraint on CN molecular spectra in laser-induced PMMA plasma [J]. *Chinese Journal of Lasers*, 2020, 47(8): 0811002.  
杨雪, 陈安民, 李苏宇, 等. 平行板约束对激光诱导 PMMA 等离子体中 CN 分子光谱的影响[J]. *中国激光*, 2020, 47(8): 0811002.
- [25] Chen J Z, Chen Z Y, Ma R L, et al. Effect of spatial confinement of carbon sheets on the soil plasma radiation characteristics [J]. *Chinese Journal of Lasers*, 2013, 40(1): 0115002.  
陈金忠, 陈振玉, 马瑞玲, 等. 碳片的空间约束对土壤等离子辐射特性的影响[J]. *中国激光*, 2013, 40(1): 0115002.
- [26] Shen X K, Sun J, Ling H, et al. Spectroscopic study of laser-induced Al plasmas with cylindrical confinement[J]. *Journal of Applied Physics*, 2007, 102(9): 093301.
- [27] Guo L B, Li C M, Hu W, et al. Plasma confinement by hemispherical cavity in laser-induced breakdown spectroscopy[J]. *Applied Physics Letters*, 2011, 98(13): 131501.
- [28] NIST Atomic Spectra Database[EB/OL]. [2021-05-01]. [http://physics.nist.gov/PhysRefData/ASD/lines\\_form.html](http://physics.nist.gov/PhysRefData/ASD/lines_form.html).
- [29] Jia R, Fu Y X, Xu P, et al. Influence of metal property on the optimized experimental parameters of laser induced breakdown spectroscopy[J]. *Journal of Atomic and Molecular Physics*, 2020, 37(5): 728-733.  
贾韧, 傅院霞, 徐鹏, 等. 金属特性对激光诱导击穿光谱最佳实验参数的影响[J]. *原子与分子物理学报*, 2020, 37(5): 728-733.
- [30] Fu Y, Hou Z, Wang Z. Physical insights of cavity confinement enhancing effect in laser-induced breakdown spectroscopy[J]. *Optics Express*, 2016, 24(3): 3055-3066.
- [31] Harilal S S, Sizyuk T, Sizyuk V, et al. Efficient laser-produced plasma extreme ultraviolet sources using grooved Sn targets [J]. *Applied Physics Letters*, 2010, 96(11): 111503.
- [32] Su X, Zhou W, Qian H. Optimization of cavity size for spatial confined laser-induced breakdown spectroscopy[J]. *Optics Express*, 2014, 22(23): 28437-28442.
- [33] Li X W, Yang Z F, Wu J, et al. Spatial confinement in laser-induced breakdown spectroscopy[J]. *Journal of Physics D: Applied Physics*, 2017, 50(1): 015203.
- [34] Fu Y T, Hou Z Y, Wang Z. Physical insights of cavity confinement enhancing effect in laser-induced breakdown spectroscopy[J]. *Optics Express*, 2016, 24(3): 3055-3066.
- [35] Sabsabi M, Cielo P. Quantitative analysis of aluminum alloys by laser-induced breakdown spectroscopy and plasma characterization[J]. *Applied Spectroscopy*, 1995, 49(4): 499-507.
- [36] Wang Y, Chen A M, Wang Q Y, et al. Influence of distance between focusing lens and target surface on laser-induced Cu plasma temperature[J]. *Physics of Plasmas*, 2018, 25(3): 033302.

# Effect of Different Numbers of Spatial Confinement Walls on Laser-Induced Cu Plasma Spectra

Dai Yuyin<sup>1</sup>, Yu Dan<sup>2</sup>, Li Yinghua<sup>1\*</sup>, Chen Anmin<sup>3</sup>, Jin Mingxing<sup>3</sup>

<sup>1</sup>*Nuclear Medicine Department, the First Bethune Hospital of Jilin University, Changchun, Jilin 130021, China;*

<sup>2</sup>*Basic Aviation College, Air Force Aviation University, Changchun, Jilin 130022, China;*

<sup>3</sup>*Institute of Atomic and Molecular Physics, Jilin University, Changchun, Jilin 130012, China*

## Abstract

**Objective** Laser-induced breakdown spectroscopy is a powerful spectroscopy technique for the analysis of various materials. As we all know, laser pulse ablates the sample and generates plasma, and the shock wave generated by the plasma propagates at supersonic speed. When the shock wave encounters the wall of confinement cavity, it will be reflected. The reflected shock wave compresses the plasma, increasing the collision rate of particles in the plasma. It will increase the number of atoms in the high-energy state and enhance the plasma's spectral intensity. As a result, many researchers have conducted extensive research on spatial confinement. However, no research group has yet investigated the effect of the number of spatial confinement walls on the spectra of laser-induced plasmas. For this reason, it is necessary to compare and study the plasma spectral emission characteristics for the different spatial confinement walls.

**Methods** We focused nanosecond laser on the surface of the Cu target to generate plasmas, and analysed the spectra of the generated plasmas. To avoid laser irradiation at the same position on the target surface, the Cu target was placed on a 3D translation stage and moved along with it. The focusing lens collected the plasma emission signal, which was then transmitted via optical fibre to a spectrometer equipped with an ICCD. To ensure time synchronisation between the laser and spectral signals, the output laser triggered the photodiode. The cavities with different spatial confinement walls (2, 3, 4, and cylindrical walls) were machined using aluminium alloy. Each spectrum was an average of 20 laser shots, and the whole experiment processes were carried out in the air.

**Results** First, the spectra for different numbers of confinement walls at a delay time of 12.5  $\mu\text{s}$  were compared. The results show that the number of confinement walls has a significant enhancement effect on the intensity of the three Cu (I) spectral lines at a delay time of 12.5  $\mu\text{s}$ . Second, the time-resolved spectral intensity of Cu (I) at 521.82 nm was measured for various numbers of confinement walls. Within the acquisition delay range of 9–22  $\mu\text{s}$ , the intensities of the Cu (I) for the number of confinement walls of 2, 3, 4, and cylindrical wall are stronger than those for the number of confinement wall of 0 (Fig. 3). The laser irradiates on the Cu target surface at the centre of the confinement cavity to generate plasma, and the shock wave generated by the Cu plasma rapidly expands (the expansion speed of the shock wave is much faster than the diffusion speed of the plasma). During the plasma expansion process, the shock wave will be reflected by the cavity wall, and the reflected shock wave will compress the Cu plasma to a smaller volume. Because energy cannot be rapidly diffused in plasma, it is absorbed by low-level atoms and transitions to the high-level, causing the intensity of the Cu (I) line to increase within the acquisition delay range of 9–22  $\mu\text{s}$ . Third, the comparison of best enhancement factors of Cu (I) at 521.82 nm for the different numbers of confinement walls at a delay time of 12.5  $\mu\text{s}$  was analyzed. It is found that when the confinement cavity is the cylindrical wall, the best enhancement factor of Cu (I) at 521.82 nm is the highest (Fig. 4). At this point, the shock wave will be reflected by the cylindrical wall, resulting in increased shock wave energy and a greater degree of coupling between the shock wave and plasma plume (Fig. 5). Fourth, the time-resolved SBR of Cu (I) at 521.82 nm for various confinement walls was measured. It is found that when the confinement cavity is the cylindrical wall, Cu (I) at 521.82 nm has the maximum SBR (Fig. 6). Finally, the time-resolved plasma temperature for the different numbers of confinement walls was calculated by the Boltzmann diagram method. Plasma temperature changes are similar to changes in spectral intensity and SBR, and the electron temperature with a confinement cavity of a cylindrical wall is the highest (Fig. 7). As previously stated, when the confinement cavity is the cylindrical wall, the spectral intensity, SBR, and electron temperature are the highest; that is to say, the spatial confinement effect is the best at this time.

**Conclusions** In this paper, the influence of the number of spatial confinement walls on laser-induced Cu plasma spectra was studied in an atmospheric environment. The experiment discovered that the spectral intensity, SBR, and electron temperature of Cu plasma increased with increasing spatial confinement walls; when the confinement cavity was the cylindrical wall, the spectral intensity, SBR, and electron temperature of the plasma were the highest. The spatial confinement effect resulted from the shock wave reflected from the confinement cavity wall compressing the plasma plume. As the number of confinement walls increased, the energy of the shock wave used to confine the plasma continued to grow, and the coupling degree of the shock wave and plasma plume was also increasing, resulting in the continuous enhancement of the compression effect of the plasma. In conclusion, it can be seen that a sufficient number of spatial confinement walls can effectively increase the spectral intensity, SBR, and electron temperature, thereby improving spectral signal and sensitivity.

**Key words** spectroscopy; laser-induced breakdown spectroscopy; the number of spatial confinement walls; spectral enhancement; electron temperature